Solution structure of moricin, an antibacterial peptide, isolated from the silkworm *Bombyx mori*

Hikaru Hemmi[a,*], Jun Ishibashi[b], Seiichi Hara[c], Minoru Yamakawa[b]

[a] *National Food Research Institute, 2-1-12 Kannondai, Tsukuba, Ibaraki 305-8642, Japan*
[b] *National Institute of Agrobiological Sciences, 1-2 Owashi, Tsukuba, Ibaraki 305-8634, Japan*
[c] *Noda Institute for Scientific Research, Noda, Chiba 278-0037, Japan*

Received 1 February 2002; revised 13 March 2002; accepted 13 March 2002

First published online 16 April 2002

Edited by Thomas L. James

Abstract A novel antibacterial peptide, moricin, isolated from the silkworm *Bombyx mori*, consists of 42 amino acids. It is highly basic and the amino acid sequence has no significant similarity to those of other antibacterial peptides. The 20 structures of moricin in methanol have been determined from two-dimensional ^{1}H-nuclear magnetic resonance spectroscopic data. The solution structure reveals an unique structure comprising of a long α-helix containing eight turns along nearly the full length of the peptide except for four N-terminal residues and six C-terminal residues. The electrostatic surface map shows that the N-terminal segment of the α-helix, residues 5–22, is an amphipathic α-helix with a clear separation of hydrophobic and hydrophilic faces, and that the C-terminal segment of the α-helix, residues 23–36, is a hydrophobic α-helix except for the negatively charged surface at the position of Asp30. The results suggest that the amphipathic N-terminal segment of the α-helix is mainly responsible for the increase in permeability of the membrane to kill the bacteria.

Key words: Antibacterial peptide; Moricin; Nuclear magnetic resonance; Solution structure; *Bombyx mori*

1. Introduction

Antibacterial peptides isolated from many kinds of insects, crustaceans, amphibians, mammals, plants, and bacteria play an important role in eliminating bacterial infections [1]. Antibacterial peptides are rapidly induced, mainly in the fat body and hemocytes, upon bacterial infection or a wounding. Insect antibacterial proteins are heat-stable and have a broad antibacterial spectrum [2]. More than 150 antibacterial peptides isolated from insects are grouped into four families [2,3]. Two of these, the cecropins and insect defensins, are well defined and relatively homogeneous: the cecropins form two α-helices and are devoid of cysteins, whereas the insect defensins contain three intramolecular disulfide bridges and consist of an α-helix linked to an antiparallel β-sheet. The two other families, the proline-rich and glycine-rich peptides/polypeptides, are heterogeneous.

Moricin, a 42-amino-acid peptide isolated from the hemolymph of the silkworm *Bombyx mori*, is highly basic and its amino acid sequence has no significant similarity to those of other antibacterial proteins [4]. Moricin has antibacterial activity against several Gram-negative and -positive bacteria. It also shows higher activity against Gram-positive bacteria than cecropin B1, a major antibacterial peptide of *B. mori*. The effects of the peptide on bacterial and liposomal membranes indicated the target of the peptide was the bacterial cytoplasmic membrane. The results also suggested that the N-terminal half of the peptide, containing the predicted α-helix, was responsible for increased membrane permeability [4]. The precise role of moricin in the immune system remains unknown, however. Moricin has an unique structural domain composed of a cluster of five basic amino acid residues in the C-terminus. It is worth determining the secondary and tertiary structure of moricin and comparing it to those of other antibacterial proteins to clarify the relationship between the unique amino acid sequence of the peptide and the antibacterial activity.

In this paper, we report the three-dimensional structure of moricin in solution determined by two-dimensional (2D) ^{1}H-nuclear magnetic resonance (NMR) spectroscopy. From the structural information, we found that moricin has an unique structure composed of a long α-helix containing eight turns over nearly the whole length of the molecule except for four N-terminal residues and six C-terminal residues. We also discuss the relationship between the unique structure of moricin and the antibacterial activity.

2. Materials and methods

2.1. Sample preparation

Recombinant moricin was efficiently produced in *Escherichia coli* as fusion proteins and released by chemical cleavage with cyanogen bromide or *o*-iodosobenzoic acid as described elsewhere [5]. This recombinant peptide has alanine instead of histidine at position 42 compared to natural moricin and shows the same antibacterial activity as that of natural moricin [5].

2.2. Circular dichroism (CD) spectroscopy

CD experiments were performed on Jasco J-720 spectropolarimeter in a 1 mm cell at 25°C. Each spectrum was the average of eight consecutive scans from 180 to 260 nm, followed by subtraction of the CD signal of peptide-free solutions. Samples were prepared by

*Corresponding author. Fax: (81)-298-387996.
E-mail address: hemmi@nfri.affrc.go.jp (H. Hemmi).

Abbreviations: CecP, cecropin P1; TFE, 2,2,2-trifluoroethanol; HFP, 1,1,1,3,3,3-hexafluoroisopropanol; CD, circular dichroism; 2D, two-dimensional; NMR, nuclear magnetic resonance; DQF-COSY, double-quantum-filtered correlated spectroscopy; TOCSY, total correlation spectroscopy; NOESY, nuclear Overhauser effect spectroscopy; RMSD, root mean square deviation

0014-5793/02/$22.00
PII: S0014-5793(02)02637-6

dissolving the peptide to the concentration of 250 μM in various solvents: water, 2,2,2-trifluoroethanol (TFE)/water solutions (from 10% to 100% (v/v) in TFE) with apparent pH from 2.3 to 3.4, and methanol.

2.3. NMR spectroscopy

A NMR sample was prepared by dissolving the recombinant peptide in 500 μl of CD_3OH (99.5%D, CIL, USA) or CD_3OD (99.8%D, Merck, Germany). Final peptide concentration was ca. 1.5 mM. All NMR spectra were obtained on Bruker Avance500 and Avance800 spectrometers with quadrature detection in the phase-sensitive mode by TPPI [6] and States-TPPI [7]. The following spectra were recorded at 20, 25, 30 and 35°C with 15 ppm spectral widths in *t1* and *t2* dimensions: 2D double-quantum-filtered correlated spectroscopy (DQF-COSY) [8], recorded with 512 and 2048 complex points in *t1* and *t2* dimensions; 2D homonuclear total correlated spectroscopy (TOCSY) [9] with DIPSI2 mixing sequence, recorded with mixing times of 35, 60, and 80 ms, 512 and 2048 complex points in *t1* and *t2* dimensions; 2D nuclear Overhauser effect spectroscopy (NOESY) [10], recorded with mixing times of 60, 100, 200, and 400 ms, 512 and 2048 complex points in *t1* and *t2* dimensions; and 2D rotating frame nuclear Overhauser effect spectroscopy (ROESY) [11], recorded with mixing time of 100 ms, 512 and 2048 complex points in *t1* and *t2* dimensions. The high digital resolution DQF-COSY and E.COSY [12] spectra were recorded using 800 and 4096 complex points in *t1* and *t2* dimensions. Water suppression was performed using WATERGATE sequence [13,14].

Slowly exchanging amide protons were determined by dissolving the lyophilized peptide in CD_3OD and collecting sequential 2-h 2D TOCSY spectra. All NMR spectra were processed using XWINNMR (Bruker). Peak-picking and assignment were performed with Sparky program (UCSF, http://www.cgl.ucsf.edu/Research/Sparky.html). Before Fourier transformation, the shifted sinebell window function was applied to *t1* and *t2* dimensions. All ^1H dimensions were referenced to internal 2,2-dimethyl-2-silapentane-5-sulfonate at 25°C.

2.4. Structure calculation

NOE-derived distance restraints were classified into three ranges, 1.8–2.7, 1.8–3.5, and 1.8–5.0 Å, according to the relative NOE intensities. Upper distance limits for NOEs involving methyl protons and non-stereospecifically assigned methylene protons were corrected appropriately for center averaging [15]. In addition, a distance of 0.5 Å was added to the upper distance limits only for NOEs involving the methyl proton [16] after correction for center averaging. Torsion angle restraints on the backbone ϕ angle were derived from $^3J_{HNH\alpha}$ coupling constants from the high digital resolution 2D DQF-COSY spectrum and intraresidue and sequential NOEs. We obtained 22 ϕ angle restraints. Backbone ϕ angles were restrained to $-60 \pm 30°$ for $^3J_{HNH\alpha} < 6$ Hz. Side-chain χ_1 angles were determined by $^3J_{H\alpha H\beta}$ coupling constants from E.COSY and short-mixing TOCSY connectivities combined with NH–Hβ and Hα–Hβ NOEs [17]. We obtained 2 χ_1 angle restraints. The χ_1 angle restraints were normally restricted to a $\pm 60°$ from staggered conformations, g+ (+60°), t (180°), or g− (−60°). Hydrogen–deuterium exchange experiments identified 25 hydrogen bond donors. Corresponding hydrogen bond acceptors were determined based on NOE patterns observed for regular secondary structural regions and preliminary calculated structures without restraints for hydrogen bonds. Hydrogen bond restraints were applied to N–H and C=O groups: 1.7–2.4 Å for the H^N–O distance and 2.7–3.4 Å for the N–O distance.

Structure calculations were performed using the hybrid distance geometry/simulated annealing method using X-PLOR 3.851 [18]. A total of 439 interproton distance restraints and 24 dihedral angle restraints were used to calculate an ensemble of structures. The structure calculation proceeded in two stages using the standard X-PLOR protocol. In the first stage, a low-resolution structure was preliminary determined using NOE-derived distance restraints and dihedral angle restraints. In the second stage, the same protocol was applied by adding hydrogen bond restraints. The force constants for the distance restraints were set to 50 kcal mol^{-1} $Å^{-2}$ throughout all the calculations, and dihedral angle restraints were initially set to 5 kcal mol^{-1} rad^{-2} during the high-temperature dynamics and gradually increased to 200 kcal mol^{-1} rad^{-2} during the annealing stage. The final round of calculations began with 200 initial structures, and the best 20 structures were selected and analyzed with MOLMOL [19], insightII (MSI, San Diego, CA, USA), and PROCHECK-NMR [20]. Structure figures were generated using MOLMOL.

3. Results

3.1. CD experiments

From the CD spectra of moricin, it was found that moricin has a largely random coil conformation in water (Fig. 1). In the presence of TFE, however, CD spectra showed two minima at 208 and 222 nm, typical of an α-helical conformation. The helical content increased with increasing the concentration of TFE up to 100% (v/v). The CD spectrum in methanol showed a spectrum very similar to that in 100% TFE, indicating that moricin adopted a maximal α-helical structure in methanol. This conformational transition from a random-coil in aqueous solution to an α-helix in hydrophobic environments such as methanol, TFE/water solution, and 1,1,1,3,3,3-hexafluoroisopropanol (HFP)/water solution is common to cecropin-like antibacterial peptides, and solution structures of cecropins and mellitin have been determined in the hydrophobic media by NMR [21–25]. The NMR structure of sarcotoxin IA, a cecropin from a flesh fly, *Sarcophaga peregrina*, has been determined in CD_3OH [21]. Therefore, NMR data were collected in CD_3OH to determine the solution conformation of moricin and compare it to tertiary structures of other antibacterial peptides, particularly cecropins.

3.2. Resonance assignment and secondary structure

Essentially complete ^1H resonance assignments were obtained for the peptide using spin system identification and sequential assignment [26] from 2D NMR spectra recorded at 20, 25, 30, and 35°C. In these assignments, Hα(i)–Hδ(i+1:Pro) (dαδ) or Hα(i)–Hα(i+1:Pro) (dαα) NOEs instead of dαN were used for Pro residues. Both proline residues, Pro4 and Pro37, showed strong dαδ NOEs, indicating that all proline residues in the peptide have *trans* configuration. Finally, the resonance assignments for the backbone and side-chain ^1H were completed except for the amide ^1H of Ala1. The resonance assignment was extended by determining stereospecific assignments of methylene protons to obtain high-precision NMR structures. Stereospecific assignments of β-methylene protons were obtained for two out of 20 residues of the peptide using information on $^3J_{H\alpha H\beta}$ coupling constants qualitatively estimated from short-mixing time TOCSY spectra combined with intraresidue NH–Hβ and Hα–Hβ NOEs. ^1H

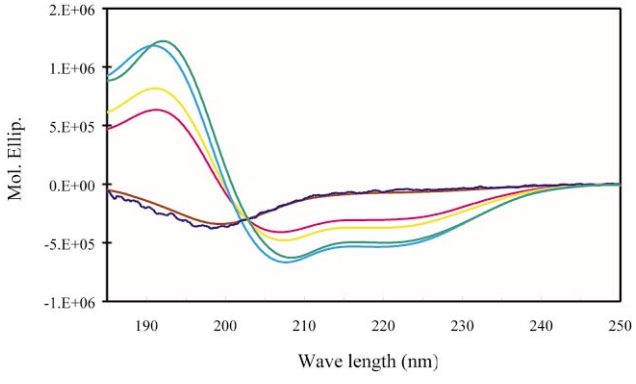

Fig. 1. CD spectra of moricin in aqueous solution (blue), in 10% TFE/water (brown), in 30% TFE/water (pink), in 50% TFE/water (yellow), in 100% TFE/water (light blue), and in methanol (green).

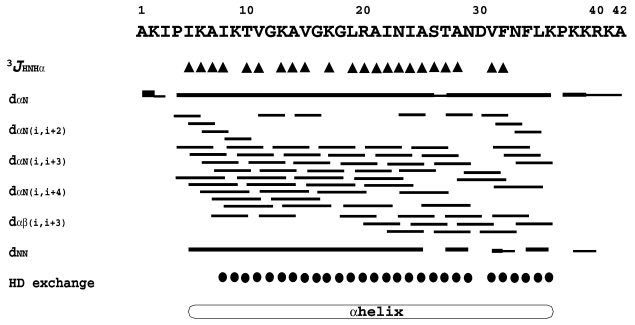

Fig. 2. Summary of the sequential NOE connectivities observed for moricin. Bars indicate NOESY cross-peaks observed between two residues. Bar height indicates NOE strength. Filled circles indicate amide protons not exchanged in 2 h after the lyophilized polypeptide was dissolved in CD_3OD. $^3J_{HNH\alpha}$ are three-bond coupling constants between HN and Hα, where the symbol represents <6.0 Hz (▲).

chemical shifts for the peptide were deposited in the BioMagResBank database under accession number 5265.

Qualitative analysis of short- and medium-range NOEs, $^3J_{HNH\alpha}$ coupling constants, and slowly-exchanging amide proton patterns was used to characterize the secondary structure of the peptide (Fig. 2). Using consecutive Hα(i)–NH(i+3), Hα(i)–NH(i+4) and Hα(i)–Hβ(i+3) NOEs, observed in the 200 ms NOESY spectrum, an α-helix was identified spanning residues Ile5 to Lys36. This α-helix is supported by the observation of a small $^3J_{HNH\alpha}$ coupling constant (<6 Hz) and amide–proton exchange data.

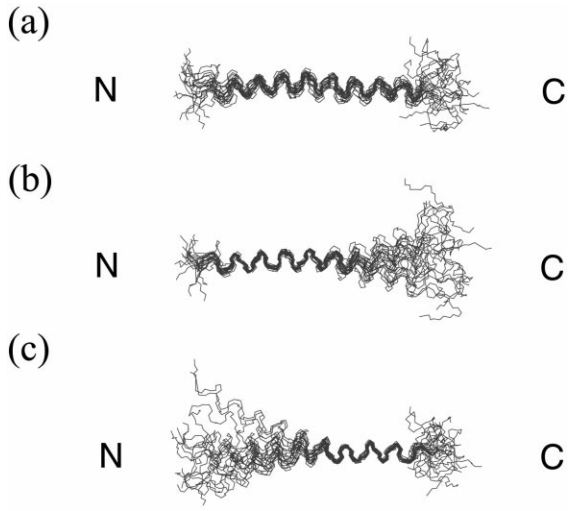

Fig. 3. Superimposition of 20 best structures of moricin with lowest total energy calculated by the hybrid distance–geometry/simulated annealing procedure of X-PLOR 3.851 [18]. These are the results of the best fit of C, N, and Cα atoms for residues 5–36 (a), for residues 5–22 (b), and for residues 23–36 (c). Only C′, Cα, and N backbone atoms are shown.

3.3. Tertiary structure of the peptide

The three-dimensional structure of the peptide was determined based on the distance and dihedral angle restraints obtained from the NMR data using the hybrid distance geometry/simulated annealing approach. A total of 200 struc-

Table 1
Statistics for best 20 NMR structures of moricin

Total restraints used	463	
Total distance restraints	439	
Intraresidue	84	
Sequential	164	
Medium ($1<\|i–j\|<5$)	141	
Long ($\|i–j\|\geq 5$)	0	
Hydrogen bond (two per bond)	50	
Total dihedral angle restraints	24	
ϕ	22	
ψ	0	
χ_1	2	
Energies (kcal/mol)[a]		
F_{total}	48.19 ± 3.574	
F_{bonds}	2.52 ± 0.465	
F_{angles}	28.76 ± 1.557	
$F_{impropers}$	2.57 ± 0.517	
F_{repel}	4.24 ± 0.953	
F_{NOE}	10.07 ± 1.635	
$F_{dihedral}$	0.025 ± 0.060	
RMSD from experimental restraints		
NOE distance restraints (Å)	0.021 ± 0.0017	
Dihedral angle restraints (°)	0.059 ± 0.1157	
RMSD from ideal covalent geometry		
Bonds (Å)	0.0019 ± 0.0001	
Angles (°)	0.386 ± 0.010	
Impropers	0.226 ± 0.023	
ϕ and ψ in most favored and additional allowed regions (%)[b]	96.7	
RMSD relative to the Mean structure (Å)		
	Backbone (N, Cα, and C′ atoms)	All non-H
Residues 5–36	1.231 ± 0.364	1.775 ± 0.282
Residues 5–22	0.576+0.252	1.330+0.242
Residues 23–36	0.584 ± 0.144	1.197 ± 0.185

[a]The final values of the square well NOE and dihedral angle potentials were calculated with force constants of 50 kcal mol^{-1} $Å^{-2}$ and 200 kcal mol^{-1} rad^{-2}, respectively. The force contacts for the van der Waals energy calculation was 4.0 kcal mol^{-1} $Å^{-4}$ with van der Waals radii set to 0.75 times the values used in the CHARMM empirical energy function.
[b]The program PROCHECK-NMR [20] was used for Ramachandran plot analysis.

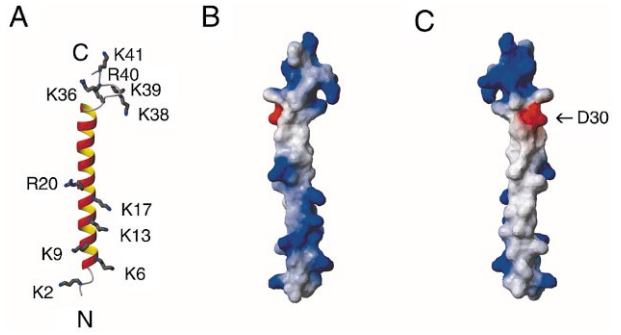

Fig. 4. The lowest energy structure of moricin among the 20 final structures. A: Ribbon diagram of moricin with side chains of basic residues shown in ball-and-stick. The helix is shown in red. B: Surface electrostatic potentials (calculated in MOLMOL [19]) of moricin orientated as in (A), colored by electrostatic potential with positive regions in blue and negative regions in red. C: Electrostatic surface as in (B) rotated by 180° about the vertical axis.

tures were calculated. Of these, 20 final structures, which showed the lowest energy values, no distance constraint violation of >0.5 Å, and no dihedral constraint violation of $>5°$, were selected. The restraints used and the structural statistics for the final structures are summarized in Table 1. The structures exhibited good covalent geometry and stereochemistry, as evidenced by the low root mean square deviation (RMSD) values for bond, angle, and improper from idealized geometry. The Ramachandran plot confirmed the high quality of the 20 structures of moricin, which showed that 96.7% of ϕ and ψ angles in moricin are found in the most favored regions and additional allowed regions, and less than 2% of ϕ and ψ angles are found in within disallowed region. The RMSDs of the 20 structures from average structure were 1.231 ± 0.364 Å for backbone heavy atoms in the region from 5 to 36, and the corresponding value is also 0.576 ± 0.252 and 0.584 ± 0.144 Å for backbone heavy atoms in the regions from 5 to 22 and from 23 to 36, respectively (Fig. 3). Coordinates were deposited in the PDB under entry code 1KV4.

Fig. 4 shows best-fit superpositions of backbone atoms of residues 5–36, residues 5–22, and residues 23–36, of the 20 converged structures of moricin. The structures show that moricin is predominantly helical, with a regular α-helix in the region from Ile5 to Lys36. The C-terminus from Pro37 to Ala42 and the N-terminus from Ala1 to Pro4 are both disordered. Because each of the entire α-helical regions is randomly bent among the 20 structures, it is not well-defined with RMSD of 1.231 Å for the backbone. In the N-terminal half of moricin, charged amino acids appear at intervals of three or four amino acid residues, indicating a characteristic structure in antibacterial proteins containing the amphipathic α-helix [27,28]. The wheel projection of amino acid residues (residues 5–22) in moricin suggested that an amphipathic α-helix formed in this region [4]. The region, residues 5–22, corresponds to the N-terminal segment of the entire α-helix and the segment is well-defined with RMSD of 0.576 Å for the backbone. The C-terminal segment of the entire α-helix, residues 23–36, is also well-defined with RMSD of 0.584 Å for the backbone. The schematic ribbon drawing and the surface representation of the structure of moricin with the lowest total energy among the final 20 structures are shown in Fig. 4. The electrostatic surface map showed that the N-terminal segment of the α-helix from Ile5 to Ile22 is an amphipathic α-helix with hydrophobic and hydrophilic faces as expected. On the other hand, the surface potentials of the C-terminal segment of the α-helix from Asn23 to Lys36 are almost hydrophobic except for the negatively charged surface structure of Asp30. The electrostatic surface map also showed that a largely positively charged surface area is located on the C-terminus of moricin, residues 36–41, due to the existence of a cluster of four basic residues.

4. Discussion

In this work, the solution structure of moricin was determined by ^{1}H NMR spectroscopy. The structure reveals an α-helix of about eight turns along nearly the full length of the molecule except for four N-terminal residues and six C-terminal residues. The N-terminal part of the α-helix, residues 5–22, is an amphipathic section, and the C-terminal of that, residues 23–36, is a hydrophobic section except for Asp30. Based on the tertiary structure consisting of an amphipathic α-helical structure and a lack of cystein in the sequence, moricin is classified to cecropin-type antibacterial peptide as previously predicted [4], even though the amino acid sequence of moricin has no significant similarity to those of other antibacterial peptides.

Cecropins are 31- to 39-residue peptides, devoid of cysteins and C-terminally amidated, and show antibacterial activity against many kinds of Gram-negative and -positive bacteria. NMR structures of two cecropins, cecropin A and sarcotoxin IA, produced by insects were determined in 15% HFP in water or CD_3OH, and consist of two amphipathic α-helices with a hinge region [21,22]. The N-terminal region is a nearly perfect amphipathic α-helix with equally large hydrophilic and hydrophobic faces. The C-terminal region is more hydrophobic. Recently the tertiary structure of cecropin isolated from the pig intestine, designated as cecropin P1 (CecP), which has 31 amino acid residues and is not amidated in the C-terminus, was determined by proton-NMR in a 30% HFP/water solution [23]. CecP is as active as insect cecropins against Gram-negative bacteria but has reduced activity against Gram-positive bacteria. The solution structure of CecP shows an elongated amphipathic α-helix over nearly the whole length of the molecule, indicating that the tertiary structure of CecP is remarkably different from the helix–hinge–helix structure of the insect cecropins. The solution structure of moricin also showed an elongated α-helix over nearly the whole length of the molecule as the first peptide of insect cecropin family, and further the α-helix of moricin is about two turns longer than that of CecP. The hinge in the helix–hinge–helix structure of the insect cecropins is due to a conserved proline residue in this family of polypeptides [29]. A similar hinge is common to several other membrane-permeating toxins such as melittin [29]. Proline has been shown to have an important role in the antibacterial activity of insect cecropins [30]. However, that the same proline was absent in CecP implied that the hinge was not essential for the antibacterial activity of CecP, at least not for Gram-negative bacteria. Recently, its proline incorporated analogue at the conserved position 22, P^{22}-CecP, was synthesized, and the analogue has reduced antibacterial activity in spite of the incorporation of the conserved proline [29]. The same proline is also absent in moricin. Hence, taking these findings together with high anti-

bacterial activity of moricin against Gram-positive and -negative bacteria, we conclude that the hinge itself is not essential for the antibacterial activity of the antibacterial peptides having an elongated α-helix against not only Gram-negative but also -positive bacteria.

Antibacterial peptides have been suggested to form voltage-dependent pores that span the cell membrane they attack [31]. The voltage-dependent pores could be formed by interaction between three or more amphipathic α-helices spanning a lipid membrane. Previously [4], we studied the effect of moricin on the permeability of the bacterial cytoplasmic membrane, finding that a target of the peptide was the bacterial cytoplasmic membrane. Further, we determined whether increased cytoplasmic membrane permeability was caused by the direct effect of the peptide on the membrane using an artificial liposome membrane with entrapped glucose. As the result, we found the change in membrane permeability was due to the direct effect of the peptide on the membrane. We also studied the effect of endoprotease Asp-N-digested fragments of the peptide on liposomal membrane permeability. The N-terminal fragment (F1), residues 1–29, released glucose from the liposome, and the releasing efficiency was about one-tenth of that of the intact peptide. On the other hand, the C-terminal fragment (F2), residues 30–42, did not release glucose from the liposome. In the fragment F1 of moricin, the existence of an amphipathic α-helix in the region, residues 5–22, was predicted by Schiffer–Edmundson wheel projection [32]. These findings suggested that the fragment F1 region of moricin containing the predicted amphipathic α-helix was responsible for increased membrane permeability, although fragment F2 was indispensable for the full expression of the antibacterial activity [4]. In this study, the solution structure of the peptide showed an α-helical structure and the N-terminal segment of the α-helix, residues 5–22, was amphipathic as expected. We conclude that the amphipathic N-terminal segment of the α-helix is the active center of moricin for antibacterial activity.

In fragment F2 of moricin, residues 30–42, there are two unique structural domains. One is half of the hydrophobic C-terminal segment of the α-helix, residues 23–36, and the other is a cluster of four basic amino acid residues in the C-terminus, residues 38–41. In the helix–hinge–helix structure of insect cecropins, both a N-terminal α-helix and a C-terminal α-helix are necessary for the full expression of antibacterial activity [22]. In pig cecropin, its proline incorporated analogue, P^{22}-CecP, has reduced antibacterial activity, which correlated with its reduced α-helical structure and its lower partitioning and membrane permeating activity with phospholipid vesicles [29]. As described above, the effect of fragment F1 on liposomal membrane permeability is much weaker than that of the intact peptide. Thus, as the α-helix of fragment F1 was shorter than that of intact peptide because of the lack of half of the hydrophobic C-terminal segment of the α-helix (residues 30–36), it is likely that the effect on liposomal membrane permeability correlates with the length of α-helical structure. These findings suggest that the C-terminal segment of the α-helix in moricin is critical for antibacterial activity. A cluster of four basic amino acid residues in moricin is notable because cecropins do not have the unique structural domain in their sequences. Most cecropins isolated from insects kill Gram-positive and Gram-negative bacteria, but CecP shows high activity only against Gram-negative bacteria [3]. Moricin has antibacterial activity against Gram-positive and -negative bacteria, and also shows higher activity against Gram-positive bacteria than cecropin B1 [4]. The surface of the bacterial membrane is negatively charged, indicating that the positively charged surface structure of the cluster of four basic amino acid residues can easily interact with the surface of bacterial membranes. Thus, it is tempting to speculate that the antibacterial specificity of moricin against bacteria is responsible for the cluster of four basic amino acid residues rather than the long α-helix containing eight turns over most of the full sequence, even though the α-helix of moricin is about two turns longer than that of CecP. To confirm this hypothesis, further study is needed of the antibacterial activity of its analogue eliminating the cluster of four basic amino acid residues in the C-terminus.

Structural information on moricin in solution thus provides a clue to understanding the precise role of moricin in the immune system.

Acknowledgements: We thank Dr. T. Kumazaki, Aomori University, for carefully reading the manuscript. This work was supported in part by the Program for Promotion of Basic Research Activities for Innovative Biosciences of the Bio-Oriented Technology Research Advancement Institution, Japan, and by a grant of Rice Genome Project PR-2110, MAFF, Japan.

References

[1] Boman, H.G. (1994) Antimicrobial Peptides. Ciba Foundation Symposium 186, Wiley, Chichester.
[2] Yamakawa, M. and Tanaka, H. (1999) Dev. Comp. Immunol. 23, 281–289.
[3] Hetru, C., Hoffman, D. and Bulet, P. (1998) in: Molecular Mechanisms of Immune Responses in Insects. (Brey, P.T. and Hultmark, D. Eds.), pp. 40–66, Chapman and Hall, London.
[4] Hara, S. and Yamakawa, M. (1995) J. Biol. Chem. 270, 29923–29927.
[5] Hara, S. and Yamakawa, M. (1996) Biochem. Biophys. Res. Commun. 220, 664–669.
[6] Marion, D. and Wüthrich, K. (1983) Biochem. Biophys. Res. Commun. 113, 967–974.
[7] Marion, D., Ikura, M., Tschudin, R. and Bax, A. (1989) J. Magn. Reson. 85, 393–399.
[8] Rance, M., Sorense, O.W., Bodenhausen, G., Wagner, G., Ernst, R.R. and Wüthrich, K. (1983) Biochem. Biophys. Res. Commun. 117, 479–485.
[9] Davis, D.G. and Bax, A. (1985) J. Am. Chem. Soc. 107, 2820–2821.
[10] Kumar, A., Ernst, R.R. and Wüthrich, K. (1980) Biochem. Biophys. Res. Commun. 95, 1–6.
[11] Griesinger, C. and Ernst, R.R. (1987) J. Magn. Reson. 75, 261–271.
[12] Griesinger, C., Sorensen, O.W. and Ernst, R.R. (1987) J. Magn. Reson. 75, 474–492.
[13] Piotto, M., Saudek, V. and Sklenar, V. (1992) J. Biomol. NMR 2, 661–666.
[14] Sklenar, V., Piotto, M., Leppik, R. and Saudek, V. (1993) J. Magn. Reson. Ser. 102, 241–245.
[15] Wüthrich, K., Billetter, M. and Braun, W. (1983) J. Mol. Biol. 169, 949–961.
[16] Clore, G.M., Gronenborn, A.M., Nilges, M. and Ryan, C.A. (1987) Biochemistry 26, 8012–8013.
[17] Wagner, G., Braun, W., Havel, T.F., Schaumman, T., Go, N. and Wüthrich, K. (1987) J. Mol. Biol. 196, 611–639.
[18] Brunger, A.T. (1993) X-PLOR Version 3.1 Mannual, Yale University, New Haven, CT.
[19] Koradi, R., Billeter, M. and Wüthrich, K. (1996) J. Mol. Graph. 14, 51–55.
[20] Laskowski, R.A., MacArthur, M.W., Moss, D.S. and Thornton, J.M. (1993) J. Appl. Crystallogr. 26, 283–291.
[21] Iwai, H., Nakajima, Y., Natori, S., Arata, Y. and Shimada, I. (1993) Eur. J. Biochem. 217, 639–644.

[22] Holak, T.A., Engstrom, A., Kraulis, P.J., Lindeberge, G., Bennich, H., Jones, T.A., Gronenborn, A.M. and Clore, G.M. (1988) Biochemistry 27, 7620–7629.
[23] Sipos, D., Andersson, M. and Ehrenberg, A. (1992) Eur. J. Biochem. 209, 163–169.
[24] Shai, Y. (1997) in: Molecular Mechanisms of Immune Responses in Insects. (Brey, P.T. and Hultmark, D. Eds.), pp. 111–134, Chapman and Hall, London.
[25] Bazzo, R., Tappin, M.J., Pastore, A., Harvey, T.S. and Carver, J.A. (1988) Eur. J. Biochem. 173, 139–146.
[26] Wüthrich, K. (1986) NMR of Proteins and Nucleic Acids, John Wiley and Sons, New York.
[27] Cociancich, S., Bulet, P., Hetru, C. and Hoffman, J.A. (1994) Parasitol. Today 10, 132–139.
[28] Kreil, G. (1994) in: Antimicrobial Peptides (Ciba Foundation Symposium 186), pp. 77–90, John Wiley and Sons Inc., Chichester.
[29] Gazit, E., Boman, A., Boman, H.G. and Shai, Y. (1995) Biochemistry 34, 11479–11488.
[30] Fink, J., Boman, A., Boman, H.G. and Merrifield, B.R. (1989) Int. J. Pept. Protein Res. 33, 412–421.
[31] Christensen, B., Fink, J., Merrifield, R.B. and Mauzerall, D. (1988) Proc. Natl. Acad. Sci. USA 85, 5072–5076.
[32] Schiffer, M. and Edmundson, A.B. (1967) Biophys. J. 7, 121–135.